ADVANCED MATERIALS
www.advmat.de

Plasmonic-Assisted Graphene Oxide Artificial Muscles

Bing Han, Yong-Lai Zhang, Lin Zhu, Ying Li, Zhuo-Chen Ma, Yu-Qing Liu, Xu-Lin Zhang, Xiao-Wen Cao, Qi-Dai Chen, Cheng-Wei Qiu,* and Hong-Bo Sun**

Muscles and joints make highly coordinated motion, which can be partly mimicked to drive robots or facilitate activities. However, most cases primarily employ actuators enabling simple deformations. Therefore, a mature artificial motor system requires many actuators assembled with jointed structures to accomplish complex motions, posing limitations and challenges to the fabrication, integration, and applicability of the system. Here, a holistic artificial muscle with integrated light-addressable nodes, using one-step laser printing from a bilayer structure of poly(methyl methacrylate) and graphene oxide compounded with gold nanorods (AuNRs), is reported. Utilizing the synergistic effect of the AuNRs with high plasmonic property and wavelength-selectivity as well as graphene with good flexibility and thermal conductivity, the artificial muscle can implement full-function motility without further integration, which is reconfigurable through wavelength-sensitive light activation. A biomimetic robot and artificial hand are demonstrated, showcasing functionalized control, which is desirable for various applications, from soft robotics to human assists.

Sophisticated motor systems of animals have been evolved to accomplish various motions, mostly through muscle contraction and relaxation around joints.[1,2] For human beings, disfunctioning muscles (e.g., hemiparesis after stroke or muscular dystrophy)[3,4] will severely damage the motility. Man-made muscle systems play a paramount role to functionalize biomimetic robots,[5–7] as well as assist the rehabilitation of those motility-disabled.[3] However, the current actuator-centric practice of artificial muscle faces great challenges for more advanced motion controls, owing to native limitations.

Certainly, actuators coupled to electric/[8,9] hydraulic/[10,11] pneumatic[5,12] circuits or built with stimuli-responsive (e.g., electricity, magnet, and light)[13–15] materials could realize deformable artificial muscles. Generally, one actuator is capable of only one specifically predefined deformation.[16,17] It cannot accomplish complex motions alone without joints. Therefore, in analogy to animals, a biomimetic motor system inevitably relies on numerous actuators to be precisely assembled with man-made skeletons and judicious coordination.[8,10] This comes with the multitudes of challenges in fabrication complexity, control strategy, and the operational cost. In the meantime, the motion control is mainly conducted in a contact fashion, e.g., those aforementioned stimuli must be physically delivered to the motor system via wired circuits,[8,18] or host materials.[10,19] Therefore, the integration problem becomes critical for many soft robots, mini robots, and facilitative equipment.

Three formidable questions naturally surface: i) Can muscle and joint merge into one identical component? ii) Can this component be remotely addressed and reconfigured without direct connections in any forms? iii) Can it be fabricated and integrated in a way that is mass-production ready?

Light-driven strategy is promising due to the free manipulation in a noncontact manner. Photothermal property is found to be an unprecedented key to those questions above.[20,21] Photothermal effects induce quite remarkably different properties among materials, such as thermal expansion,[22,23] trans–cis transition,[24,25] and hydrophilicity–hydrophobicity transition.[11,26] Thermal expansion is a ubiquitous phenomenon that is promising in broad application. Herein, we report a uniform bilayer configuration made of Au nanorods embedded in graphene oxide (AuNRs@GO) and poly(methyl methacrylate) (PMMA), enabling a light-sensitive artificial muscle to perform complex limb-like motions without joints literally. Such "holistic artificial muscle" (HAM) tailors the promising nature of light-responsive materials,[15,27–29] leading to control the strength of contraction/expansion through the plasmonic-assisted actuation under laser exposure with different wavelength.

The physical mechanism behind such rapid local deformation under light activation could be interpreted as follows.

B. Han, Prof. Y.-L. Zhang, L. Zhu, Y.-Q. Liu, X.-L. Zhang, X.-W. Cao, Prof. Q.-D. Chen, Prof. H.-B. Sun
State Key Laboratory of Integrated Optoelectronics
College of Electronic Science and Engineering
Jilin University
2699 Qianjin Street, Changchun 130012, China
E-mail: yonglaizhang@jlu.edu.cn

Dr. Y. Li, Prof. C.-W. Qiu
Department of Electrical and Computer Engineering
National University of Singapore
Kent Ridge, Singapore 117583, Republic of Singapore
E-mail: chengwei.qiu@nus.edu.sg

Dr. Z.-C. Ma, Prof. H.-B. Sun
State Key Laboratory of Precision Measurement Technology and Instruments
Department of Precision Instrument
Tsinghua University
Haidian district, Beijing 100084, China
E-mail: hbsun@tsinghua.edu.cn

The ORCID identification number(s) for the author(s) of this article can be found under https://doi.org/10.1002/adma.201806386.

DOI: 10.1002/adma.201806386

Graphene possesses high thermal conductivity and excellent mechanical strength; however, GO has rather poor thermal properties due to the destruction of ordered sp^2 domain.[30,31] The final configuration could thereby be designed by local photoreduction of GO using laser scribing,[32] which changes GO to reduced GO (RGO). More importantly, graphene and its derivatives (here GO and RGO) have very small or even negative coefficients of thermal expansion (CTEs),[33,34] in the radical contrast with the positive CTE of PMMA. Upon photothermal heating, the mismatch between the deformations of two layers leads to significant bending, replicating the muscle-like contraction from one layer and expansion from the other. AuNRs play a significant enabler's role to enhance light/heat conversion efficiency within RGO layer due to surface plasmon resonance,[35,36] and then transfer the heat effectively to raise the temperature of PMMA layer through localized heating of RGO layer. Some other noteworthy consequences include: 1) the aspect ratio of AuNRs could be a new dimension to manipulate their plasmonic resonant wavelengths and thereby such HAM can be functionalized or deactivated by selected wavelength of the driving laser; and 2) such HAM is thereby free of any joints during bending.

Limb motion is one essential type of animal's motions.[1] Natural muscles cannot achieve such segmented motion without the structure of joints (**Figure 1**a), but artificial muscles can be much more versatile and powerful with directly laser-printed HAM (Figure 1b). The addition of AuNRs with various plasmonic absorption peaks can tailor the strength of grip and hence control the function of the robot. With the plasmonic-reprogrammable strategy,[37,38] the artificial muscle can be applied for different purposes, e.g., a light-assisted hand as shown in Figure 1c. The bending areas are actually synthesized by the bilayer HAM, instead of traditional joints. This mechanism can also be directly adopted to realize a mini robot (such as a spider robot in Figure 1d). Such mini robots get rid of component-assembly procedures, since the whole process is composed of laser scribing and addressing.

The spider robot with patterned nodes was fabricated through a classical laser-scribing method (**Figure 2**a).[32] A LightScribe-enabled DVD was coated with PMMA and AuNRs@GO nanocomposite in sequence, forming a bilayer structure. After drying at ambient conditions, laser scribing was used to write thermal conductive nodes on the AuNRs@GO layer according to computer-designed patterns (Figure S1, Supporting Information). The bilayer film was then peeled off the DVD and the spider pattern was cut along its boundary, thus creating a light-driven robot.

The longitudinal surface plasmon resonance (LSPR) of AuNRs can be synthetically tailored across a broad spectral range.[35,39] The light-absorption properties of AuNRs@RGO can be correspondingly controlled to match the specific wavelength of light stimuli (Figure S2, Supporting Information). The simulation of a single AuNR shows an enhancement of the electric field on the nanorod surface (Figure 2b), and thus a high light-to-heat conversion efficiency would be expected (Figure 2c). The plasmonic effect of AuNRs greatly facilitates the follow-up photoreduction of GO and light-addressable configuration. Electrostatic interaction causes the AuNRs to disperse homogeneously on the GO sheet (Figure 2d). The AuNRs@GO nanocomposite is a photocurable material that can be effectively reduced and patterned using very weak near-infrared lasers or even a standard LightScribe DVD optical drive (focused 790 nm laser, 5 mW). After laser scribing, clear RGO patterns are observable by naked eyes (Figure 2e). The RGO layers evidence

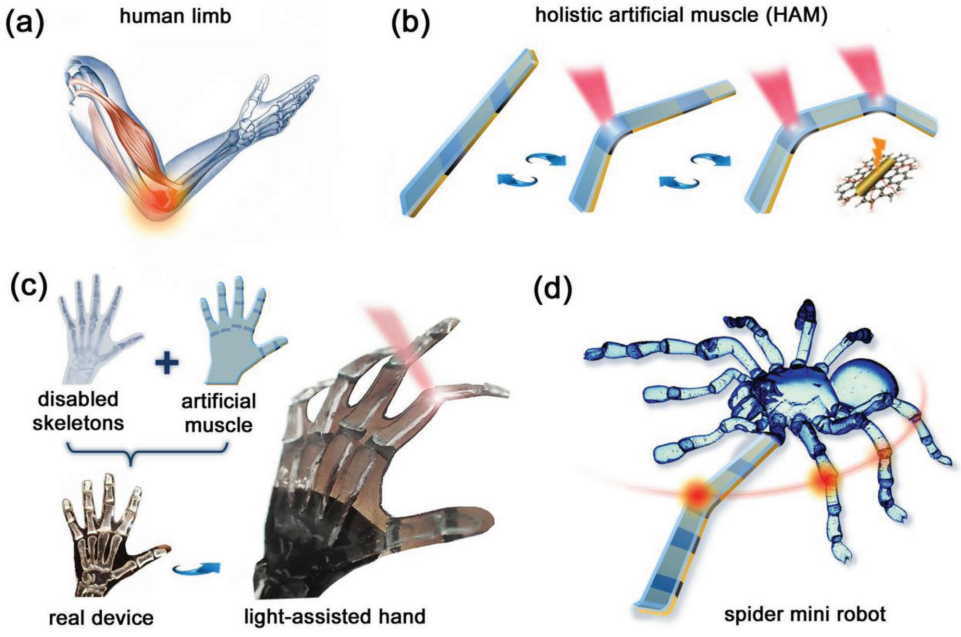

Figure 1. Design of the HAM. a) A human arm whose motions are accomplished through a combined work of muscles and skeletons. b) Schematic illustration of the patterned artificial muscle. Light induces deformations of the HAM, which can be selectively activated. c) A hand can accurately assist its motions using light, see Movie S1 in the Supporting Information for the performance of a real device. d) A spider mini robot can be directly fabricated using the artificial muscle, without further assembling.

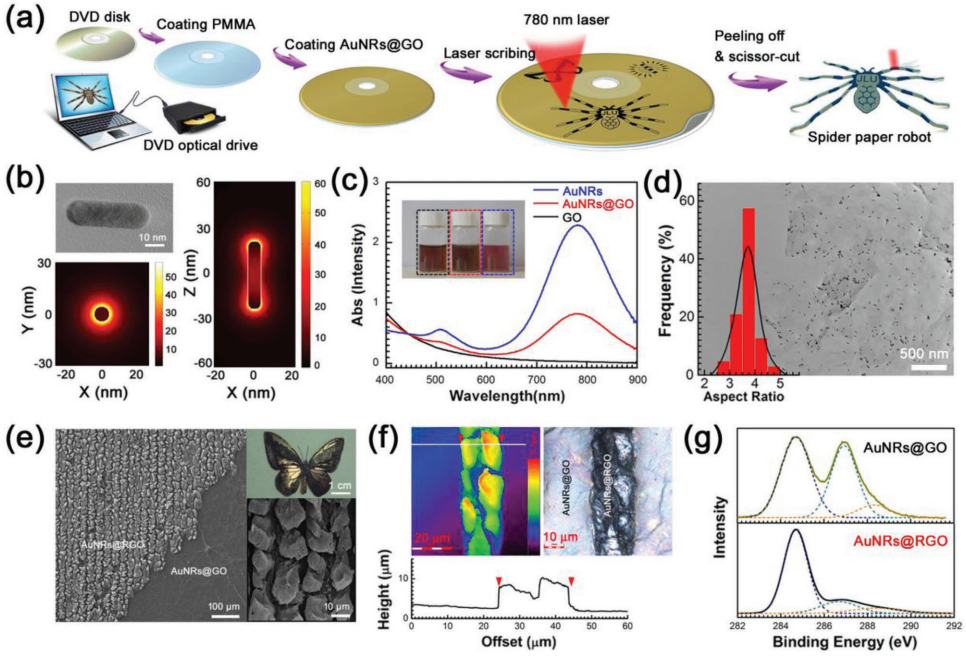

Figure 2. Fabrication procedure of bio-inspired graphene oxide robot. a) Schematic of the fabrication and driving mechanism of a bio-inspired robot. b) TEM image of a single AuNR and the COMSOL simulation of electric field enhancement. The color bars represent the ratio between the enhanced electric field and the incident electric field (no unit). It could be enhanced up to 60 times in the vicinity of AuNRs. c) UV–vis absorbance spectra reveal that combining AuNRs with GO can well inherit the light absorption properties of the two components (wavelength-selective absorption of AuNRs and the broadband absorption of GO). The inset shows photographs of aqueous solutions of GO, AuNRs@GO, and AuNRs, respectively. d) TEM image of AuNRs@GO nanocomposite. The inset chart shows the aspect ratio distribution of AuNRs. e) Top-view SEM image of nanocomposite material before (AuNRs@GO) and after (AuNRs@RGO) laser-scribing treatment. The top right inset shows a sample of laser-scribed butterfly, and the bottom right inset shows the magnified SEM image of the AuNRs@RGO area. f) Laser scanning confocal microscopy image of the microstructure of a single line treated by the laser scribe method, indicating the resolution could reach 20 μm and the height was 10 μm taller than untreated region. g) C1s XPS spectra of AuNRs@GO (top) and AuNRs@RGO (bottom). Most of the oxygen groups (C—O and C=O) have been removed.

the expansion and exfoliation, which could be attributed to the degassing process during the removal of oxygen-containing groups. In the bilayer structure, the AuNRs@RGO layer has a tunable photoreduction by adjusting the content of AuNRs (Figure S3, Supporting Information). Laser scanning confocal microscopy has been employed to investigate the topography change, confirming the expansion of the RGO layer (Figure 2f). The resolution of feature size could reach 20 μm, which is sufficient to create light-driven nodes for sophisticated robot design. X-ray photoelectron spectroscopy (XPS) confirmed the photoreduction of GO (Figure 2g and Figure S3e,f, Supporting Information). The photoreduction degree and the thickness of the composite layer further depend on the amount of AuNRs; much higher C/O ratio can be achieved with more AuNRs (Figure S4, Supporting Information). In this way, we successfully developed light-addressable robots without further integration using a cost-effective method.

To quantitatively evaluate the plasmonic-induced photothermal effect before and after laser scribing, we patterned a Taiji diagram that consists of AuNRs@GO and AuNRs@RGO on a PMMA film and used an infrared camera to measure the temperature change across the diagram (**Figure 3**a). In the photothermal images, the pattern was clearly visible due to the different temperature changes upon light irradiation. For example, under the irradiation of a 200 W filament lamp, the PMMA substrate keeps its temperature almost constant, whereas the temperature of the AuNRs@RGO region increased by ≈35 °C, over two times more than that of the AuNRs@GO region. The rapid temperature rise of the AuNRs@RGO/PMMA bilayer strip (<0.1 s, Figure 3b) is attributed to its high optical absorbance property and excellent thermal conductivity. The photothermal effect of the surface plasmon resonance contributes to the high light-to-heat conversion efficiency, and therefore facilitates the fast response. The maximum temperature change shows an approximately linear relationship with light intensity (Figure 3c). We found that the temperature of the AuNRs@RGO region rises nearly twice as much as that of the AuNRs@GO region. Since the temperature rise directly causes the expansion of the PMMA layer, the dependence of maximum bending curvature of the bilayer strip on laser intensity follows a similar tendency (Figure S5, Supporting Information). The curvature model presents a linear relationship with the temperature increment ($\rho = C\Delta T$, see Simulation of the HAM models, Figure S6, and Table S1 in the Supporting Information for details); thereby, the bending curvature of the laser-treated region is dominant. Dynamic photothermal analysis of bilayer strips under 50 mW cm^{-2} light irradiation indicates rapid bending of RGO-based materials (Figure 3d). The AuNRs@RGO/PMMA bilayer strip takes only 0.05 s to reach the curvature of 76 m^{-1}, whereas the AuNRs@GO/PMMA strip takes 0.6 s. Compared to various light-driven strategies (photothermal expansion, *trans–cis* transition, and

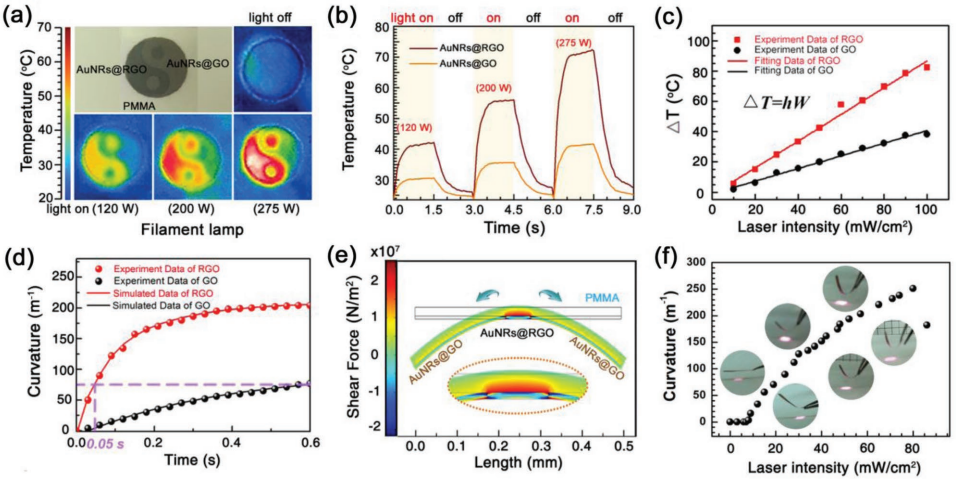

Figure 3. Characterization of the photothermal actuators. a) Infrared images of films comprising three materials under different levels of irradiation from a filament lamp. b) Temperature measurement of AuNRs@GO and AuNRs@RGO film as filament lamp of different power intensities. c) Temperature changes of RGO and GO bilayer strips as a function of laser intensity. The RGO-fitting heat transfer coefficient (h) is nearly two times higher than that of GO materials. d) Dynamic analysis of curvature under 50 mW cm^{-2} laser irradiation as a function of time. The simulation data matches the experimental data. e) COMSOL simulation of simplified HAM model by imposing temperature changes on the structure. The inset shows the distribution of inner forces at the intermediate position. f) Experimental results of simple HAM sample for the maximum bending curvature as a function of laser intensity.

hydrophilicity–hydrophobicity transition), the response time of our HAM is much shorter.[24–26] This prompt response to laser addressing is preferential for the design of the artificial muscle. The energy conversion efficiency of AuNRs@RGO/PMMA is nearly 50 times higher than that of AuNRs@GO/PMMA and nearly 300 times higher than that of other carbon-based actuators without AuNRs (see Energy conversion of photothermal segment actuators in the Supporting Information for details).[27] We simulated the internal stress distribution for a given temperature variation on such a patterned bilayer structure (Figure 3e). In our model, the bilayer structure consists of a PMMA layer and a composite layer of AuNRs@GO. In the middle of the composite layer, GO has been reduced to RGO. Temperature variation can induce different thermal strains in the two layers: the PMMA layer bears a compressive force, while the composite layer sustains a tensile force. To balance these forces, the bilayer structure bends. Since the laser reduction of GO significantly increases the thermal conductivity and light absorption of the composite, the HAM sample bends more in the laser-treated region. The maximum bending curvature of HAM shows a strong dependence on the light intensity (Figure 3f). Under intense light irradiation (80 mW cm^{-2}), the maximum curvature can reach ≈250 m^{-1}. The bending force also follows a similar tendency; it increases with the input light intensity, reaching ≈60 mN under 80 mW cm^{-2} irradiation (Figure S7, Supporting Information). Inspired by this effect, patterned ribbons can be designed to form a specific configuration (letters J, L, and U) upon filament lamp irradiation (Figure S8, Supporting Information). The flexible patterning of photothermal-responsive nodes unfolds a potential roadmap to design and fabrication of biomimetic motor systems.

In order to verify the plasmonic-affected wavelength-selective response, we used three kinds of AuNRs with central absorption wavelengths of 533, 637, and 813 nm, respectively (**Figure 4**a). Under the stimulation of 405, 532, 635, and 808 nm lasers, the maximum temperature changes showed strong correlation with the size of AuNRs (Figure 4b). The strips bent only when the absorption band of the AuNRs was close to the laser wavelength and then outgoing enough heat and bending energy. This perfect wavelength selectivity is beneficial to the light-addressable performance for complex robot design. Here, an artificial finger combined with different size of AuNRs at various joints shows excellent light-sensitive actuation performance (Figure 4c and Figure S9, Supporting Information). The nanoparticles play an important role in controlling the output elastic energy and strength of bending, thus enabling precise manipulation of robots.

The flexible printing capability of laser scribing makes it highly accessible to the potential mass production of HAM that can be manipulated using different light sources, such as filament lamps and laser beams with specific wavelengths. The HAM can bend over 16 000 times under light irradiation without degradation (Figure S10, Supporting Information). The average bending force was maintained at 50 mN for 50 cycles. The reversible response properties (bending curvature) showed no obvious degradation over 20 months, which is stable enough for biomimetic motor system. As typical examples, a set of hand skeletons made from poly(dimethylsiloxane) (PDMS) is integrated with a prepatterned HAM (**Figure 5**a,b). In this way, the plasmonic-assisted hand can be manipulated by laser in a non-contact manner (Figure 5c). Every node could bend freely under laser irradiation, indicating the light-addressable manipulation (Movie S1, Supporting Information). For a relative complex robot design, a Venus flytrap robot enabled by HAM is demonstrated. Natural Venus flytrap consists of a pair of terminal lobes hinged at the midrib where the lobes fold to form the trap. The edges of the two lobes are fringed by cilia, which mesh together to prevent prey from escaping. According to this prototype, we design and printed a Venus flytrap robot, in which the midrib and the cilia region have been reduced into AuNRs@RGO to

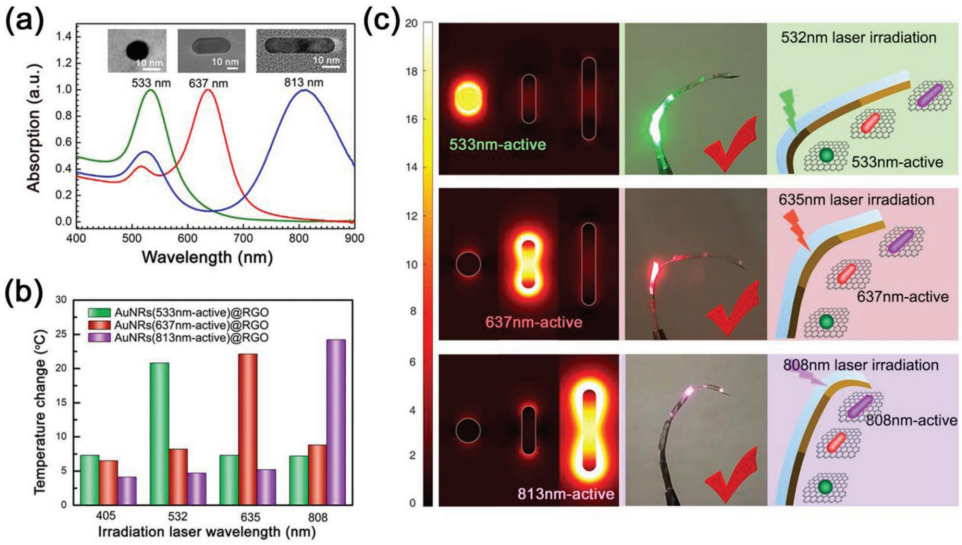

Figure 4. Wavelength selective properties by doping with different AuNRs. a) Normalized absorption spectra of different aspect ratio AuNRs, corresponding to LSPR shifts from 500 to 900 nm. The maximum absorption peaks center at 533, 637, and 813 nm. b) Maximum temperature variation of HAMs prepared using different AuNRs (with central absorption peaks of 533, 637, or 813 nm) under the stimulation of lasers with wavelengths of 405, 532, 635, or 808 nm. Every excitation laser is calibrated to maintain the same transmitted power of ≈50 mW cm^{-2}. c) Simulation of electric field enhancement of three different AuNRs and corresponding response of ribbons with three different HAM active to lasers of 532, 635, or 808 nm wavelength.

get better photothermal response, whereas the rest region is AuNRs@GO (Figure 5d,e). By switching a filament lamp on and off, we can prompt the Venus flytrap robot to perform reversible capture and release actions (Figure 5f; Movie S2, Supporting Information). To demonstrate the light-addressable manipulation of complicated multiped robot, a holistic spider robot has been developed. Each leg of the spider has been patterned with three nodes (Figure 5g). Despite that the spider has been patterned on 2D film, it can deform into 3D structures under light irradiation due to the bending of its legs. When the

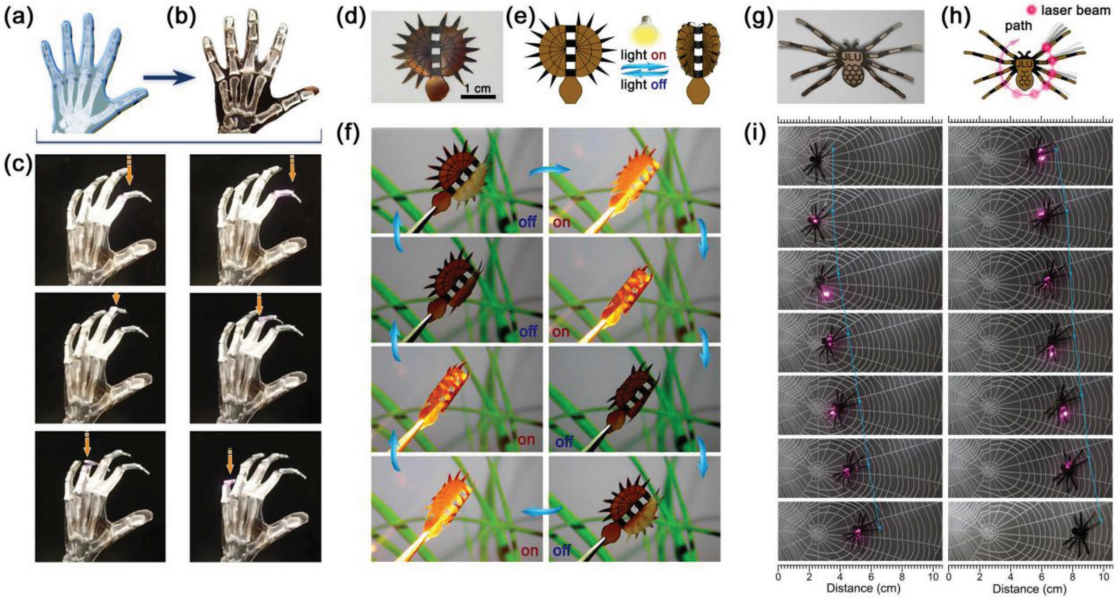

Figure 5. HAM-enabled mini robots. a–c) Light-assisted hand. a) Schematic illustration of a light-assisted hand fabricated by integrating a set of disabled hand skeletons (PDMS) with HAM. b) Photograph of a real device. c) Light-addressable manipulation of the HAM-enabled hand in different situations. d–f) Light-responsive Venus flytrap robots. d) Schematic illustration of light-driven Venus flytrap. Midrib and fringed cilia were reduced, that could curl dramatically; areas where GO was not reduced curled slightly. e) Photograph of the Venus flytrap robots. f) Light manipulation of the Venus flytrap robot. The flytrap can capture or release something by simply switching the light on and off. g–i) Manipulation of a HAM-enabled spider robot. g) Photograph of the spider mini robot. h) Schematic illustration for the light-addressable manipulation. i) Light-driven walking of the spider robot. The infrared laser irradiates on the leg, and the local heating induced bending of the leg, leading to the displacement of the gravity center and moving forward.

laser beam irradiates the leg one by one, the legs bend one after another, which induced the displacement of the gravity center of the spider accordingly. In this way, we could control the spider robot to lean forward and move toward the right direction at an average speed of 2.5 mm s^{-1} (Figure 5h,i and Movie S3, Supporting Information). It can walk freely through remote manipulation using one or more laser beams (see Driving forces of the spider robot in the Supporting Information for details). Actually, light-driven HAMs are not limited to the aforementioned examples. The fast and reversible response of the flexibly printed photothermal actuators enables the rational design of various light-driven robots with ultralow cost (≈5.7 cent for one spider robot, see Production cost of the spider robot in the Supporting Information for details) for remote manipulation.

In summary, we propose a plasmonic-assisted HAM that can independently act as a full-functional motor system without assembling or joints. The artificial muscle has a low-cost integrated design consisting of a composite layer (AuNRs@GO and AuNRs@RGO) and a thermally expansive polymer layer (PMMA). With the aid of a standard LightScribe drive, programmable photothermal patterns can be printed onto these layers efficiently and massively. AuNRs of varying aspect ratios endow the nanocomposites with tunable wavelength response. We have demonstrated light-assisted hand and robots as proof-of-concept prototypes. The present work bridges the gap between ideal request and realistic restrictions of biomimetic motor systems, and decreases the amount of discrete parts, the number of post-processing steps, and the fabrication time, and thereby offers new opportunities for biological aid and for biomimetic mini robot to be remotely operated at enclosed harsh environment.

Experimental Section

Preparation of AuNRs@GO/PMMA Bilayer Films: 4 g PMMA (Sigma-Aldrich Co.) was dissolved in 12 mL ethyl acetate (Sigma-Aldrich Co.) by magnetically stirring at 35 °C for 4 h. The PMMA film was made by spin-coating at 1500 rpm for 20 s; the average thickness of the PMMA film was 15 µm. The GO was prepared using an improved Hummer's method by oxidation of natural graphite powder (Aldrich, <150 µm). The intermolecular forces were destroyed through oxidization and the GO was washed with deionized water for several times before use. The prepared AuNRs (1 M, 0.2 wt%) were mixed with GO (1 M) solution with a volume ratio of 1:10 and stirred for at least 1 h, ensuring the AuNRs were incorporated homogeneously onto the GO sheets by electrostatic interaction. 5 mL AuNRs@GO composite was cast onto PMMA films (2 cm × 2 cm) and dried in a ventilated area, forming AuNRs@GO and PMMA bilayer structures. During the drying process of AuNRs@GO solution, the water molecules evaporated from the top of surface, thus forming a concentration gradient in the thickness direction and ultimately preset a shear stress between two layers. Therefore, a curved bilayer film was obtained when it was peeled off from the DVD disk.

Patterning of the AuNRs@GO/PMMA Bilayer Films Using LightScribe Technology: This LightScribe reduction method requires neither high temperatures nor toxic chemicals and thereby could be easily used at home. A 780 nm focused near-infrared laser was integrated within a DVD drive, through which one could easily modify what was written on the disc via a computer-controlled program. In addition, one could write on the same DVD repeatedly, and it could be used to perform the large-scale, rapid, and maskless reduction of AuNRs@GO composite materials. It took only 20 min to completely reduce a layer of GO that covered an entire DVD. The AuNRs@GO/PMMA film was fixed onto a LightScribe-enabled DVD and deposited into the DVD drive. Certain patterns (such as butterfly, dragonfly, honeybee, ant, and spider) were programmed into the LightScribe control panel. Through irradiation of the laser integrated in the DVD drive for about 20 min, the AuNRs@GO/PMMA film was reduced into AuNRs@RGO/PMMA according to the predesigned pattern (Figure S1, Supporting Information).

The mass ratio of AuNRs to GO was adjusted from 0 with respect to pure GO to ≈0.05. By changing the concentration of AuNRs, the RGO layer showed tunable thicknesses of 2–10 µm (Figure S3, Supporting Information), corresponding to different degrees of reduction of AuNRs@GO, through the same process as described in the "Preparation of AuNRs@GO/PMMA bilayer film." Besides, the bending behavior and force also depended on the amount of AuNRs. According to the experimental results, a mass ratio of AuNRs/GO at ≈0.04 is considered as an optimized composition (Figure S11, Supporting Information). Scanning electron microscopy (SEM, JEOL JSM-7500F, and Japan) was utilized to measure the surface morphologies of the samples. Notably, there were many cracks and pores distributed on the surface of the RGO, which could be attributed to the degassing of oxygen-containing groups. The chemical compositions of the specimens were characterized by XPS (ESCAL-AB250, VG Microtech, UK). In order to analyze the degree of reduction of different AuNRs-containing samples, the XPS of GO and the resultant AuNRs@RGO composites were measured. The oxygen signals decreased dramatically as the amount of AuNRs increased (Figure S3e,f, Supporting Information). The significantly reduced oxygen content indicated that the AuNRs@GO films were effectively reduced through the AuNR-induced photothermal effect.

Bending Performance of AuNRs@GO/PMMA and AuNRs@RGO/PMMA Bilayer Strips: To compare the AuNRs@GO/PMMA and AuNRs@RGO/PMMA bilayer strips actuation under the same light irradiation intensity, the AuNRs@GO/PMMA and AuNRs@RGO/PMMA bilayer strips (2 mm × 20 mm) were suspended in air with one end fixed to a glass rod. The strips were exposed to filament light (100 W) with a distance of 30 cm. The temperature changes on the surface were measured through a thermal infrared imager (FLIR ONE, USA), which was set 15 cm right in front of the samples. When the strips bent to their maximum, images were taken by an Olympus camera in the lateral direction 10 cm away from the samples. The bending angles were measured using a protractor that compared to the initial state.

Temperature Measurement of AuNRs@GO/PMMA and AuNRs@RGO/PMMA Pattern: The Taiji diagram was created using aforementioned LightScribe technology. The pattern was extracted and the remaining area was wiped with knife blade making the PMMA layer exposed to light at the same time for comparison. An infrared camera was positioned 10 cm away from the film surface. The temperature of the diagram was recorded as rising rapidly before reaching a steady value. The temperature changes varied between different materials; the Taiji diagram became clearer under light irradiation (Figure 3a).

Synthesis and Characterization of AuNRs with Different Aspect Ratio: Gold nanorods were prepared by modifying the previously described seed-mediated growth method.[40] First, the seed solution was prepared by adding 0.25 mL $HAuCl_4$ (0.01 M) to 7.5 mL cetyltrimethyl ammonium bromide (CTAB) solution (0.1 M); $HAuCl_4$ was used as a precursor and CTAB acted as a cationic surfactant. Then 0.6 mL ice-cold $NaBH_4$ (0.01 M) was added with vigorous stirring of the solution for 1 min. The color of the solution changed from light yellow to brownish yellow within a few seconds. The seed solution was stirred continuously for at least 2 h for subsequent use. To prepare the growth solution, 200 mL CTAB (0.1 M) was mixed with 11.2 mL chloroauric acid ($HAuCl_4$; 0.01 M) at 28 °C, 2.8 mL silver nitrate ($AgNO_3$; 0.01 M) was added to this solution with gentle stirring, and 1.6 mL ascorbic acid ($C_6H_8O_6$; 0.1M) was added dropwise. The volume of $AgNO_3$ determined the morphology of the gold nanorods. The mild reduction of ascorbic acid changed the solution from dark brown to colorless. Finally, 0.8 mL of the seed solution was added to the growth solution, initiating the growth of AuNRs. The temperature of the solution was kept constant at 28 °C for 12 h. The pure AuNRs were created after purifying the solution by centrifugation at 8000 rpm three times. The AuNRs were isolated in the precipitate, and excess reactant was removed. The aspect ratios of the prepared

nanorods were around 3.75. The absorption spectra of the nanorods were investigated by UV–vis spectrometer (UV-2550, SHIMADZU) in the 400–900 nm range. The peaks of the transverse and longitudinal surface plasma resonance were located at 511 and 782 nm, respectively. When different volumes of silver ions were added to the growth solutions, the LSPR of the AuNRs shifted from 530 to 1000 nm. The AuNRs whose LSPR peaks centered at 533, 537, and 813 nm were used in this study, by adding $AgNO_3$ (0.01 M) to growth solutions with volumes of 0, 1.4, and 2.8 mL, respectively. High-resolution transmission electron microscopy (TEM, JEOL JEM-2100F, Japan) images of synthetic nanorods were taken at 200 kV. For each sample, 200 particles were measured to determine the average size distribution (Figure S2, Supporting Information). In order to achieve the wavelength-selective manipulation, the gold nanorods with different absorption wavelengths were diluted using deionized water to make sure they possess identical absorption value. Then the obtained solutions were mixed with GO respectively to prepare three different kinds of AuNRs@GO composites.

Measurement of the Blocking Force: The actuator was suspended on the aluminum block with one end fixed and the other free on the surface (see inset of Figure S7, Supporting Information). Tin foils (24 g m^{-2}) of different size (weight) were used to measure the bending force. If the actuator could just lift the Sn foil, its gravity was equal to the blocking force.

Fabrication of Light-Assisted Hand Model: The hand bones were first made through laser cutting of PDMS film (2 mm in thickness). Since there was no joint system supporting the integration, bones were separated from each other. After a holistic artificial hand muscle was pasted onto the bones precisely, the disabled bones were able to functionalize as a whole. The model showed 12 flexible nodes, which are integrated through one-step laser scribing approach. The laser was set 30 cm away from the model, assisting the finger activities through a noncontact manner.

Supporting Information

Supporting Information is available from the Wiley Online Library or from the author.

Acknowledgements

This work was supported by the National Key Research and Development Program of China and the National Natural Science Foundation of China (NSFC) under Grants #2017YFB1104300, #61590930, #61775078, #61522503, and #61435005.

Conflict of Interest

The authors declare no conflict of interest.

Keywords

gold nanorods, graphene oxide, light-driven actuators, plasmonic effect, soft robotics

Received: October 3, 2018
Revised: November 3, 2018
Published online: December 9, 2018

[1] M. H. Dickinson, C. T. Farley, R. J. Full, M. A. R. Koehl, R. Kram, S. Lehman, *Science* **2000**, *288*, 100.
[2] F. C. Anderson, M. G. Pandy, *J. Biomech. Eng.* **2001**, *123*, 381.
[3] C. D. Takahashi, L. Der-Yeghiaian, V. Le, R. R. Motiwala, S. C. Cramer, *Brain* **2008**, *131*, 425.
[4] E. Mercuri, F. Muntoni, *Lancet* **2013**, *381*, 845.
[5] M. Wehner, R. L. Truby, D. J. Fitzgerald, B. Mosadegh, G. M. Whitesides, J. A. Lewis, R. J. Wood, *Nature* **2016**, *536*, 451.
[6] R. Kempaiah, Z. Nie, *J. Mater. Chem. B* **2014**, *2*, 2357.
[7] C. Tawk, M. In Het Panhuis, G. M. Spinks, G. Alici, *Soft Robot.* **2018**, https://doi.org/10.1089/soro.2018.0021.
[8] S. R. Shin, B. Migliori, B. Miccoli, Y. C. Li, P. Mostafalu, J. Seo, S. Mandla, A. Enrico, S. Antona, R. Sabarish, T. Zheng, L. Pirrami, K. Zhang, Y. S. Zhang, K. T. Wan, D. Demarchi, M. R. Dokmeci, A. Khademhosseini, *Adv. Mater.* **2018**, *30*, 1704189.
[9] T. Someya, Z. Bao, G. G. Malliaras, *Nature* **2016**, *540*, 379.
[10] T. Ranzani, S. Russo, N. W. Bartlett, M. Wehner, R. J. Wood, *Adv. Mater.* **2018**, *30*, 1802739.
[11] H. Yuk, S. Lin, C. Ma, M. Takaffoli, N. X. Fang, X. Zhao, *Nat. Commun.* **2017**, *8*, 14230.
[12] D. Rus, M. T. Tolley, *Nature* **2015**, *521*, 467.
[13] K. Y. Ma, P. Chirarattananon, S. B. Fuller, R. J. Wood, *Science* **2013**, *340*, 603.
[14] W. Hu, G. Z. Lum, M. Mastrangeli, M. Sitti, *Nature* **2018**, *554*, 81.
[15] O. M. Wani, H. Zeng, A. Priimagi, *Nat. Commun.* **2017**, *8*, 15546.
[16] Y. Liu, B. Shaw, M. D. Dickey, J. Genzer, *Sci. Adv.* **2017**, *3*, e1602417.
[17] A. M. Abdullah, X. Li, P. V. Braun, J. A. Rogers, K. J. Hsia, *Adv. Mater.* **2018**, *30*, 1801669.
[18] M. Kaltenbrunner, T. Sekitani, J. Reeder, T. Yokota, K. Kuribara, T. Tokuhara, M. Drack, R. Schwodiauer, I. Graz, S. Bauer-Gogonea, S. Bauer, T. Someya, *Nature* **2013**, *499*, 458.
[19] K. Ariga, T. Mori, J. P. Hill, *Adv. Mater.* **2012**, *24*, 158.
[20] B. Han, Y. L. Zhang, Q. D. Chen, H. B. Sun, *Adv. Funct. Mater.* **2018**, *28*, 1802235.
[21] D. Li, D. Han, S.-N. Qu, L. Liu, P.-T. Jing, D. Zhou, W.-Y. Ji, X.-Y. Wang, T.-F. Zhang, D.-Z. Shen, *Light: Sci. Appl.* **2016**, *5*, e16120.
[22] F. Li, H. Hou, J. Yin, X. Jiang, *Sci. Adv.* **2018**, *4*, eaar5762.
[23] M. Amjadi, M. Sitti, *ACS Nano* **2016**, *10*, 10202.
[24] M. Lahikainen, H. Zeng, A. Priimagi, *Nat. Commun.* **2018**, *9*, 4148.
[25] T. Ube, K. Kawasaki, T. Ikeda, *Adv. Mater.* **2016**, *28*, 8212.
[26] C. Ma, W. Lu, X. Yang, J. He, X. Le, L. Wang, J. Zhang, M. J. Serpe, Y. Huang, T. Chen, *Adv. Funct. Mater.* **2018**, *28*, 1704568.
[27] X. Zhang, Z. Yu, C. Wang, D. Zarrouk, J. W. Seo, J. C. Cheng, A. D. Buchan, K. Takei, Y. Zhao, J. W. Ager, J. Zhang, M. Hettick, M. C. Hersam, A. P. Pisano, R. S. Fearing, A. Javey, *Nat. Commun.* **2014**, *5*, 2983.
[28] H. Yang, W. R. Leow, T. Wang, J. Wang, J. Yu, K. He, D. Qi, C. Wan, X. Chen, *Adv. Mater.* **2017**, *29*, 1701627.
[29] R. L. Lawrence, B. Scola, Y. Li, C.-K. Lim, Y. Liu, P. N. Prasad, M. T. Swihart, M. R. Knecht, *ACS Nano* **2016**, *10*, 9470.
[30] W. Xiong, Y. S. Zhou, W. J. Hou, L. J. Jiang, Y. Gao, L. S. Fan, L. Jiang, J. F. Silvain, Y. F. Lu, *Sci. Rep.* **2015**, *4*, 4892.
[31] M. Acik, G. Lee, C. Mattevi, M. Chhowalla, K. Cho, Y. J. Chabal, *Nat. Mater.* **2010**, *9*, 840.
[32] M. F. El-Kady, V. Strong, S. Dubin, R. B. Kaner, *Science* **2012**, *335*, 1326.
[33] S. Wang, M. Tambraparni, J. Qiu, J. Tipton, D. Dean, *Macromolecules* **2009**, *42*, 5251.
[34] D. Yoon, Y.-W. Son, H. Cheong, *Nano Lett.* **2011**, *11*, 3227.
[35] M. Kauranen, A. V. Zayats, *Nat. Photonics* **2012**, *6*, 737.
[36] A. F. Zedan, S. Moussa, J. Terner, G. Atkinson, M. S. El-Shall, *ACS Nano* **2013**, *7*, 627.
[37] M. E. Nasir, S. Peruch, N. Vasilantonakis, W. P. Wardley, W. Dickson, G. A. Wurtz, A. V. Zayats, *Appl. Phys. Lett.* **2015**, *107*, 121110.
[38] D. Floess, J. Y. Chin, A. Kawatani, D. Dregely, H.-U. Habermeier, T. Weiss, H. Giessen, *Light: Sci. Appl.* **2015**, *4*, e284.
[39] L. Rosa, K. Sun, V. Mizeikis, S. Bauerdick, L. Peto, S. Juodkazis, *J. Phys. Chem. C* **2011**, *115*, 5251.
[40] B. Nikoobakht, M. A. El-Sayed, *Chem. Mater.* **2003**, *15*, 1957.